금속표면처리
Journal of the metal finishing society of Korea
Vol. 17. No. 2, Jun. 1984
〈연구논문〉

ALLOY STRUCTURE AND ANODIC FILM GROWTH ON RAPIDLY SOLIDIFIED AL-SI-BASED ALLOYS

H.S. Kim,** G.E. Thompson, G.C. Wood, I.G. Wright* and R.E. Maringer*

Corrosion and Protection Centre, UMIST, Manchester, UK.
**Battelle Laboratories, Columbus, OH, U.S.A.*
***University of Ulsan, Korea*

ABSTRACT

The structure of rapidly solidified Al-Si-based alloys and its relationship to subsequent anodic film growth in near neutral and acid solutions have been investigated. Solidification of the alloys proceeds via pre-dendritic nuclei, associated with rugosity of the casting surface, from which cellular-type growth, comprised of aluminium-rich material surrounded by silicon-containing material, emanates.

Observation of ultramicrotomed sections of the alloys and their anodic films reveals the local oxidation of the silicon-rich phase and its incorporation into the anodic alumina film, formed in near neutral solutions. Such incorporation occurs but resultant isolation of the silicon-rich phase is not possible for anodizing in phosphoric acid, and a three-dimensional network of the oxidized silicon-containing phase, with continuing development of porous anodic alumina, is observed.

INTRODUCTION

The modification of alloys and their surfaces by special techniques to improve their corrosion and oxidation and wear resistance has received relatively widespread interest recently. For example, high corrosion resistance is observed for metal-metalloid glasses (Fe-Cr-P-C alloys) produced by rapid solidification from the melt (1), relatively high dose ion implantation into metals has been used for persistent oxidation resistance (2) and resistance to intergranular attack is possible by laser glazing of the surface of 304 stainless steel (3). In addition, novel high strength to weight ratio materials, with beneficial properties extending to higher than normal temperatures, have been developed by compaction of rapidly solidified powders (Al-Fe-Mo alloys) (4). These techniques, in addition to co-vacuum deposition, and thus available to develop non-equilibrium alloys with altered surface conditions and, dependent on alloy composition and the technique employed, differing extents of crystalline and amorphous material. Of these techniques, rapid solidification and co-vacuum deposition allow production of 'bulk'

alloys (often relatively thin strips), whereas laser treatment and ion implantation rely on modified surface and near surface regions respectively.

In order to understand the novel materials and to develop further alloys that may be exploited commercially, in-depth analytical studies, based on further insight into the resultant material substructure, its relationship, if any, to the composition of the air-formed/thermal/passive/anodic film and likely flaw distribution are necessary. Additionally, examination of nonequilibrium alloys may give important insight into the major factors governing the behaviour of conventional materials.

Such a study is made here, employing rapidly solidified Al-Si and Al-Cu-Si alloys chill cast onto a rotating copper wheel to produce 'bulk' materials requiring, at least for this study, no further fabrication/compaction. Analytical transmission electron microscopy of ultramicrotomed sections of the alloys and their attached films has been used extensively to allow direct observation and fine analysis of the alloy substructure and its influence on subsequent anodic film growth in appropriate solutions.

EXPERIMENTAL PROCEDURE

An Al-10wt% Si alloy and an Al-8.5% Si-3.5% Cu alloy were chill cast onto the surface of a rotating copper wheel (Batelle Laboratories, Columbus, Ohio) to produce continuous ribbons of the individual 'bulk' alloys of thickness about 200 and 100 μm respectively. The resultant alloys were then anodized after degreasing in acetone, with no further surface preparation; occasionally strips of the Al-10% Si alloy were heat-treated at 673K for various times to determine the effect on the distribution of phases in the alloy and on subsequent anodic film growth.

Spade electrodes, prepared in the usual manner (5), were anodized at constant current density in near neutral ammonium pentaborate solution and phosphoric acid; the progress of anodizing was followed by monitoring the resultant voltage-time behaviour.

Generally, the alloys and their films were observed in a Philips EM301 transmission electron microscope; electron transparent sections of the alloys and their attached films, about 50nm thickness, parallel to the electron beam, were prepared by ultramicrotomy using a DuPont Sorval ultramicrotome (6). Analytical transmission electon microscopy was carried out in a Philips EM 400 instrument with EDX facilities (Joint UMIST/University of Manchester Department of Metallurgy).

Structure of the rapidly solidified Al-based alloys.

Clearly by developing a thin ribbon of alloy foil from the single rotating wheel, two surfaces are developed, the *wheel-side surface* and the *upper surface* remote from the wheel. Direct examination of the respective surfaces, by optical microscopy and scanning electron microscopy, revealed little evidence of any structural features; hydration of the air-formed film, developed over the macroscopic alloy surfaces during storage, and its subsequent cracking during drying out in the vacuum of the scanning electron microscope were evident.

In order to reveal any features at the respective alloy surfaces, several surface treatments were carried out including etching, electropolishing and anodizing at relatively low current density in phosphoric acid at 295K. The last treatment was very effective in giving good contrast and creating a three-dimensional effect at the surface through film growth, as found by others (7) and, since anodizing was a feature of this study, its use for surface structure revelation was continued. Scanning electron micrographs of the respective surfaces of the Al-10% Si alloy, illustrated in Fig. 1, reveal various features of interest, which are considered further below:

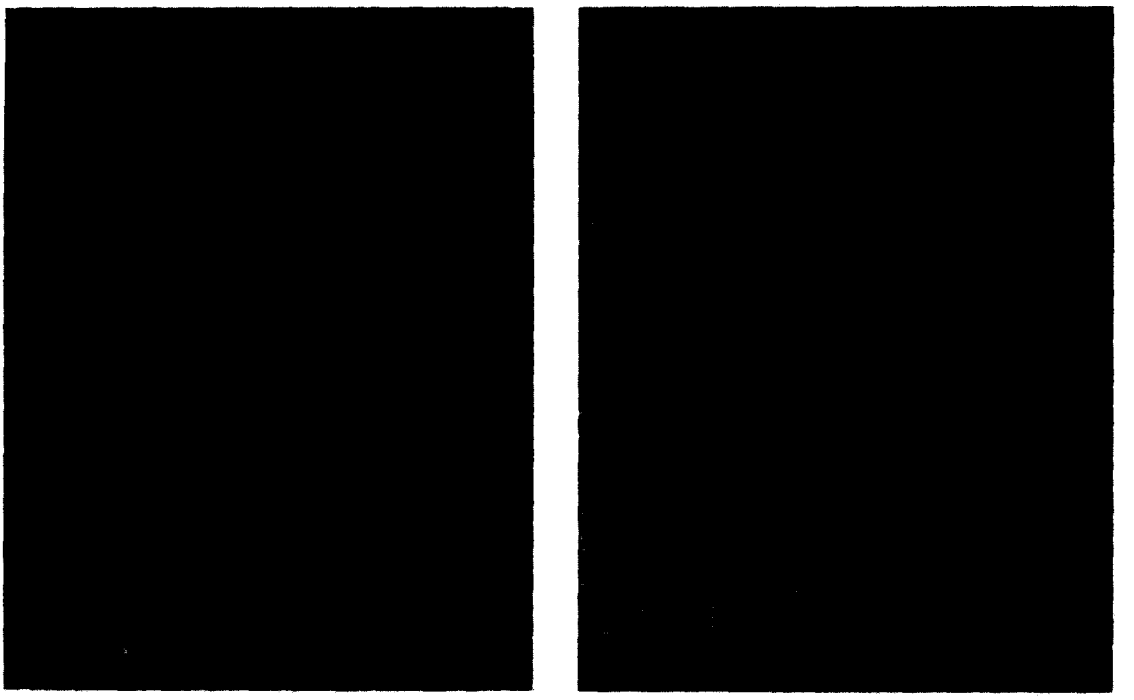

Figure 1. Scanning electron micrographs of the surfaces of the rapidly solidified Al-10% Si alloy : (a) Wheel-side surface; (b) Upper surface.

(i) At the wheel-side surface 'grains' are evident, of diameters in the range of 10-30μm, and their boundaries are decorated by an apparently light phase.

(ii) Within the grains at the wheel-side surface, finely-spaced lamellae (0.4-0.6μm) composed of adjacent dark and light phase, running generally parallel to the surface of the alloy foil are evident. Close scrutiny of the surface micrograph shows that the lamellae appear to emanate from a central, relatively diffuse region within the grain (Fig. 2).

(iii) For the upper surface, remote from the wheel, a generally cellular texture is evident, comprising of relatively dark material surrounded by the light phase; a wide distribution of cells is apparent, with effective diameters in the range of 0.6-2.9μm.

Generally similar features are observed for the respective surfaces of the Al-8.5% Si-3.5% Cu alloy, with the interlamellar spacing at the wheel-side surface being in the range 0.5-0.7μm and the cellular texture of the upper surface having effective diameters in the range of 0.5-1.7μm.

In order to understand further the change from lamellae-like structure within grains of the alloy at the wheel-side surface to the cellular texture at the upper surface, remote from the wheel, a transmission electron microscopy examination of appropriate specimens, prepared by ultramicrotomy, has been carried out.

Particular advantages of ultramicrotomy in this study relate to its ability to generate electron transparent sections without preferential removal of phases, relatively precise location of the sections of the materi-

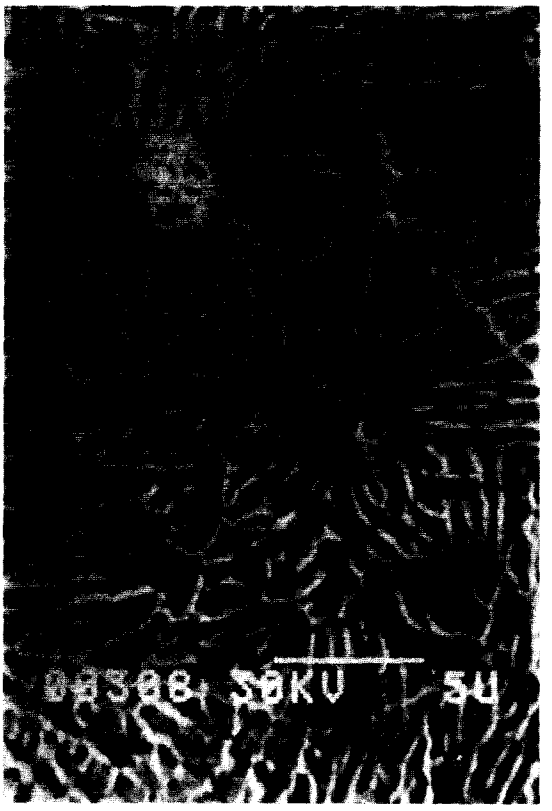

Figure 2. Scanning electron micrograph of the wheel-side surface of the rapidly solidified Al-10% Si alloy, showing relatively diffuse regions from which apparent lamellae emanate.

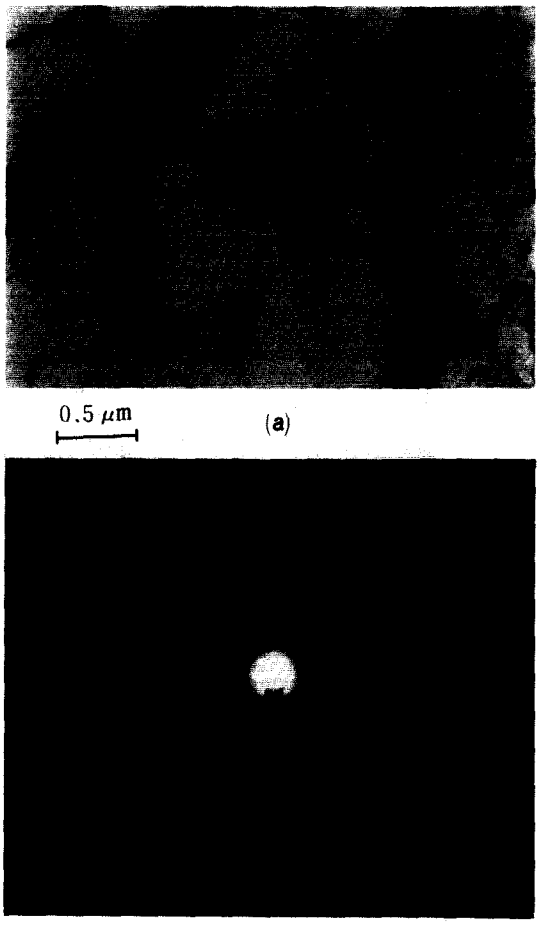

Figure 3. Transmission electron micrograph of an ultrami crotomed section of the Al-10% Si alloy, perpendicular to the wheel-side surface and (b) the typical electron diffraction pattern showing relatively broad rings associated with the silicon-containing phase superimposed on the single crystal pattern from the alumium - rich phase.

al, and sections perpendicular to the surfaces examined by SEM may be produced.

A transmission electron micrograph of an ultramicrotomed section, perpendicular to the wheel side surface, is shown in Fig. 3.

Typical features revealed in the micrograph are crystalline regions of material, showing extinction contours at their particular orientations to the electron beam, surrounded by a relatively brittle 'second phase-type' material. The relatively brittle nature of the latter phase is assessed from the fine chatter bands, arising from mechanical damage due to sectioning, and typically evident in second phase material in aluminium and its alloys. The effective diameter of the

crystalline region is in the range of 0.5 to 1μm and the width of the enveloping material varies between 50-1000°A.

Selected area electron diffraction of the respective region within the section indicates that the crystalline regions are f.c.c, with a lattice parameter in the range 4.03 to 4.07°A close to aluminium(4.05°A).The 'second-phase' material, enveloping the crystalline region, shows an electron diffraction pattern typical of a polycrystalline, perhaps microcrystalline, material of lattice parameter about 5.4°A (Fig. 3b).

Energy dispersive analysis of X-rays (EDX), using a nominal electron probe size of about 100A, to optimize spatial resolution and X-ray counts, has been employed to confirm the above findings. With the probe positioned with the 'aluminium' regions, silicon was detected at just above background levels. On the other hand, for the probe positioned within the silica-containing material, singificant yields of aluminium and silicon were detected.

Use of the Cliff-Lorimer expression (8) to determine the concentrations of silicon and aluminium within the respective regions gives typically the following levels:

Aluminium-containing region: 1wt% Si; remainder Al

Silicon-containing region: 60wt% Si; 40% Al.

Taking into account the effective diameter of the regions analyzed, likely beam spreading and the detection limits of the technique, it is clear that relatively low levels of silicon are present within the aluminium-rich phase. For the silicon-rich phase, relatively high levels of aluminium were detected, a significant fraction of which may have been generated from the adjacent aluminium-rich grains because of the relatively low effective width of the silicon-rich phase compared to the nominal probe diameter and its enveloping circle of confusion in which significant X-ray generation may proceed.

Comparison of ultramicrotomed sections from near the wheelside and upper-side surfaces suggests that aluminium-rich regions of approximately hexagonal appearance and near [100] zone axis are not evident near the upper-side surface, where elongated aluminium-rich regions, of near [110] zone axis, are almost exclusively encountered.

For the Al-8.5% Si-3.5% Cu alloy, a generally similar appearance, of aluminium-rich regions and the enveloping silicon-rich phase. is evident, as seen for the Al-10% si alloy. The composition of the phases, determined by EDX, is given below:

WHEEL-SIDE SURFACE

Aluminium-containing region:

2.9wt% Si; 1.3% Cu; 0.2% Mn; remainder Al

Silicon-containing region:

47.9wt% Si; 6.7% Cu; 0.8% Mn; 3.6% Fe; 41% Al

UPPER SURFACE

Aluminium-containing region:

2.3wt% Si; 1.2% Cu; 0.2 Mn; 0.2% Fe; remainder Al

Silicon-containing region:

35.2wt% Si; 7.2% Cu; 1.2% Mn; 4.2% Fe; 52% Al

At face value, the aluminium-rich phase contains up to about 3% Si and 1% Cu, with relatively low levels of impurities (Fe and Mn). The silicon-containing phase shows relatively large levels of iron and copper, and significant yields of aluminium, although probe spreading into the adjacent regions cannot be discounted. In addition, there appears to be little variation in the composition of the aluminium-rich phase from the wheel-side surface to the upper-side surface. On the other hand, the silicon-containing phase shows a reduction in silicon content towards the upper surface; the

significance, or otherwise, of this analysis requires further clarification with smaller electron probes, positioned entirely within the silicon-containing phase.

Anodic Film Growth on the Al-Si Based Alloys

Anodizing by conventional methods and hard anodizing of cast Al-Si based alloys are normal commercial practices for corrosion and wear resistance respectively (9). However, for the rapidly solidified alloys employed in this study, the relatively fine distribution of the aluminium and silicon-containing phases allows an almost unique opportunity to observe directly the likely competing processes of anodic film growth over the aluminium-rich phase and 'flaws' comprising silicon-containing material, which intersect the macroscopic surface and/or are revealed as the metal/film interface recedes during anodizing.

Barrier-type anodic film formation

The typical voltage-time curve generated for anodizing the Al-10% Si alloy at a constant current density of $100 Am^{-2}$ in 5wt% ammonium pentaborate solution at 298K is illustrated in Fig. 4. The voltage increased relatively slowly with time over the initial 10 min of anodizing; subsequently, the voltage increased more rapidly with time, eventually reaching a maximum value of about 400V. A relatively copious evolution of gas bubbless, probably oxygen, was detected during the initial period of slow voltage increase which decreased during the relatively rapid region of voltage increase with time. Finally, electroluminescence was observed during anodizing, detected at voltages above 50V and increasing in intensity from 80V; from about 350V, sparking was evident over the macroscopic alloy surface indicating the onset of dielectric breakdown during anodizing.

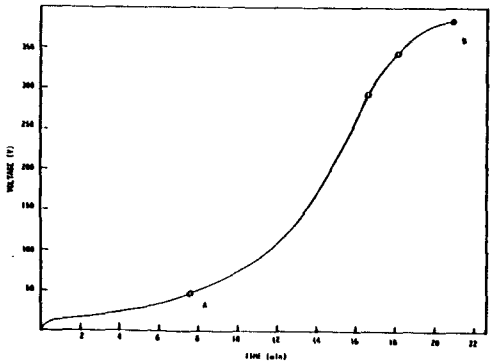

Figure 4. Voltage-time behaviour for anodizing the Al-10% Si alloy at a constant current density of $100 Am^{-2}$ in 5 wt% ammonium pentaborate solution at 298 K.

A transmission electron micrograph of an ultramicrotomed section of the anodic film formed to 300V, under the conditions of Fig. 4, is illustrated in Fig. 5. The alloy substrate is evident at the bottom of the micrograph with the anodic film material passing

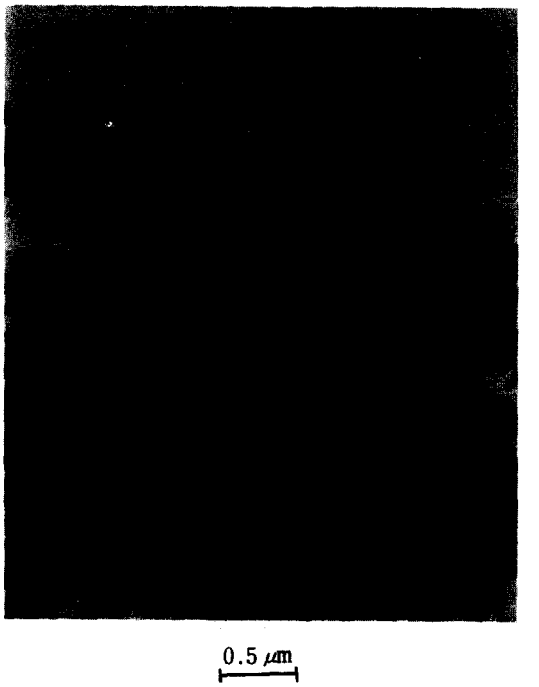

Figure 5. Transmission electron micrograph of the ultramicrotomed section of Al-10% Si alloy and the anodic film, formed to 300V under the conditions of Fig. 4.

parallel to the alloy/film interface. The anodic film appears relatively irregular, with undulating alloy/film and film/solution interfaces; additionally local textured regions are apparent within the usually featureless anodic alumina.

The local textured regions are situated within the film material at positions above and/or adjacent to the silicon-containing networks in the alloy substrate; between the silicon-containing networks, the aluminium-rich phase/film interface appears scalloped. The total anodic film thickness is in the range 3814-4576A° the former value giving a forming ratio of about 12.7A° which is greater than that expected for anodizing relatively pure aluminium under similar conditions.

Anodizing of the Al-8.5% Si-3.5% Cu alloy showed a similar voltage-time response and the presence of electroluminesecence.

Porous-type anodic film formation

The voltage-time behaviour observed for anodizing the Al-10% Si at various constant current densities, in the range 20-200Am^{-2}, in 0.4M phosphoric acid at 300K is illustrated in Fig. 6. Generally, the voltage is seen to increase relatively rapidly at the commencement of anodizing to a peak or plateau voltage, beyond which a steady-state region is evident; with increase in applied current density, an increase in the steady-state voltage is observed. The general behaviour is thus typical of anodizing aluminium in acid solutions but, as indicated in Fig. 6, the voltages achieved for anodizing of the alloy are markedly reduced compared with anodizing of aluminium under the same conditions.

Illuminating insight into the alloy behaviour during anodizing is given in the transmission electron micrograph of the ultramicrotomed section of the film formed at 20Am^{-2} for 20 min, where a steady-state voltage of about 12V was achieved (Fig. 7a). A relatively regular, fine-featured, porous anodic film has developed above the aluminium-rich phase whereas,

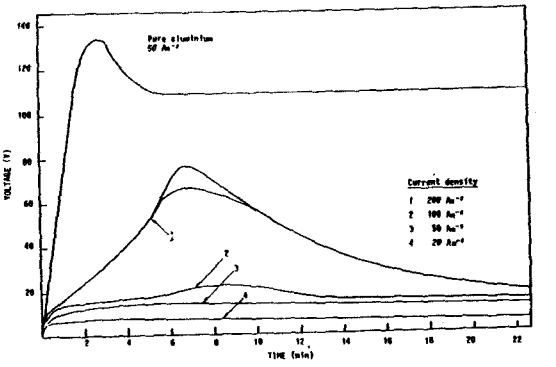

Figure 6. Voltage-time behaviour for anodizing the Al-10% Si alloy at various current densities in 0.4M phosphoric acid at 300K.

apparent anodic oxidation of the silicon-containing network, originally present at the substrate surface, has resulted in the local development of a product, which appears to spread laterally, parallel to the alloy/film interface of the adjacent anodic alumina film material.

A transmission electron micrograph of an ultramicrotomed section of the Al-8.5% Si-3.5% Cu alloy, anodized at 200Am^{-2} in 0.25M phosphoric acid at 295K for 30 minutes to a steady state voltage of about 15V, is illustrated in Fig. 7b.

Here, apparently similar anodizing behaviour to the Al-10% Si alloy has occurred with porous anodic film formation over the aluminium-rich phase and anodic oxidation of the silicon-containing phase; generally the 'anodic film' appears to comprise an open three-dimensional network of the anodized silicon phase, with apparently dispersed regions of anodic alumina, through the film sections. Thus, the alloys show broadly similar types of anodic film growth above the respective regions, which are considered further in the discussion; subtleties introduced into the anodizing behaviour through the presence of copper are not considered further.

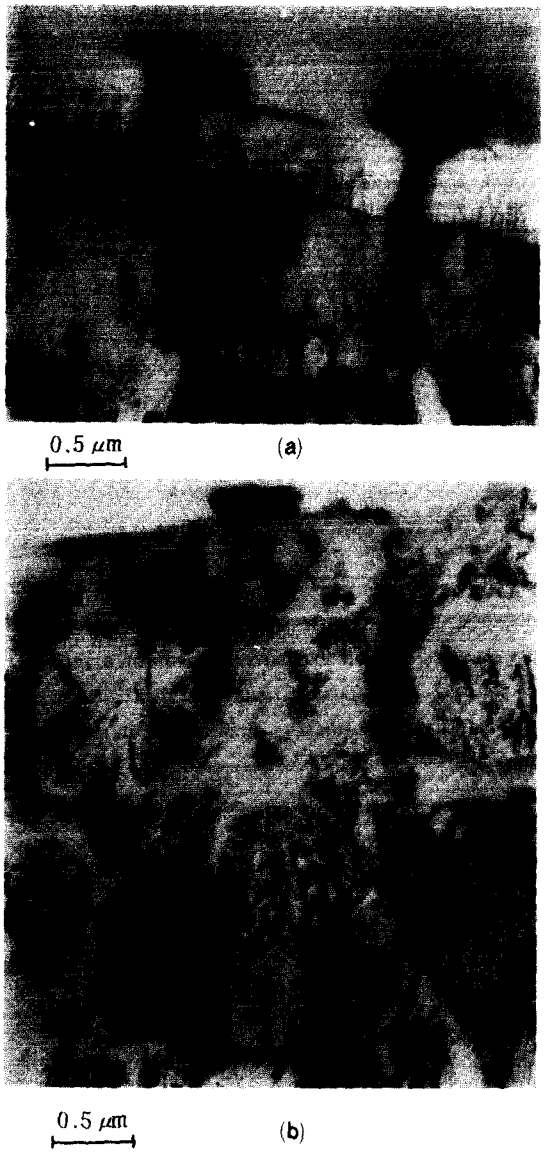

Figure 7. Transmission electron micrographs of ultra-microtomed sections of the rapidly solidified alloys and their anodic films: (a) Al-10% Si alloy anodized at $20Am^{-2}$ in 0.4M phosphoric acid for 20 min at 300K; (b) Al-8.5% Si-3.5 %Cu alloy anodized at $200Am^{-2}$ in 0.25M phosphoric acib for 30min at 295K.

Heat treatment of the Al-10% Si and subsequent anodic film formation

Heat treatment of the rapidly solidified Al-10% Si alloy for 8h at 673K results in the almost complete change of the silicon-containing networks to discrete regions of silicon, with relatively large particles present of effective diameters in the range 1.2-2.0μm; an increase in ductility of the relatively brittle alloy accompanies the redistribution of the silicon-containing phase. The change of the distribution of the silicon-containing networks with time of heat treatment at 673K is reflected in the voltage time response on subsequent anodizing at $100Am^{-2}$ in 0.4M phosphoric acid at 295K (Fig. 8). Generally, with increase of time of heat

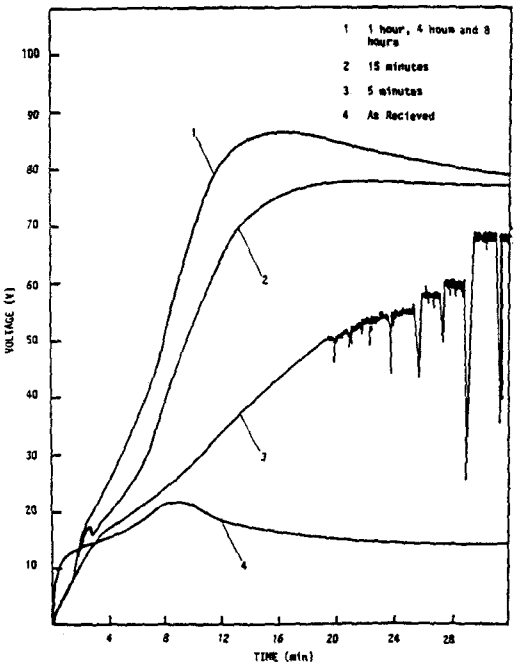

Figure 8. Voltage-time behaviour for anodizing the Al 10% Si alloy, after various times of heat treatment at 673K, at $100Am^{-2}$ in 0.4M phosphoric acid at 295K.

treatment, the voltage achieved at a particular anodizing time increases; after heat treatment for 8h, a voltage time response generally similar to that of aluminium is evident, although again, the voltage monitored for the alloy at any stage of anodizing is less than that for aluminium at the corresponding time. Partial explanation of this behaviour is evident in the ultramicrotomed section of the heat treated alloy which has been anodized (Fig. 9). The development of discrete particles of silicon from the silicon-containing networks has led to internal porosity within the alloy, with electrolyte access to relatively gross silicon particles, such that anodic film development proceeds in such regions during anodic polarization.

Figure 9. Transmission electron micrograph of the ultramicrotomed section the Al-10% Si, heat treated for 8h at 673K, and its film formed at 200Am ^{2} in 0.4M phosphoric acid.

DISCUSSION

Alloy Substructure

The general appearance of the rapidly solidified Al-Si and Al-Si-Cu alloys is similar, with apparent grains and fine lamellae evident at the wheel-side surface and a cellular appearance of phase revealed at the upper side surface, remote from the wheel. This variation of the apparent phase distributions may be rationalized by considering initial solidification at the relatively cool, rotating copper wheel, with its good heat transfer characteristics. Points of local contact of the melt with the copper wheel exhibit predendritic solidification, as found in chill castings (10), such that local nucleation and subsequent growth proceed in a relatively smooth spherical front, with the solute content of the melt remaining unchanged. These local regions are apparent in Fig. 1, as the diffuse regions of relatively dark appearance. Over distances of about 1.5 to 3μm from the centres of the regions of nucleation, the spherical nucleation disappears and lamellae-type development emanates, generally associated with microsegregation of solute. Evidently, lamellae-type development is seen at the wheel-side surface with cellular-type development at the upper surface. In reality, lamellae-type development is a manifestation of cellular-type growth, but viewed normal to the axis of the cell. A schematic illustration of the solidification of the alloy is depicted in Fig. 10, showing the radial development of the cells from the pre-dendritic nuclei of solidification, and the preferred growth directions revealed from ultramicrotomed sections of the alloy; the diagram depicts only primary dendrites developing from pre-dendritic nuclei and does not indicate the presence of secondary dendritic arms which are present in the appropriate scanning and transmission electron micrographs. Grains and their boundaries, apparently revealed at the wheel-side surface, then merely represent merging of cells developing from their respective nuclei, in a plane parallel to the wheel-side surface.

An empirical relationship (11) exists between dendritic spacing and cooling rate which, for an Al-11% Si alloy, is linear on a log-log scale,

i.e. $\lambda = \beta \dot{\varepsilon}^{1/3}$

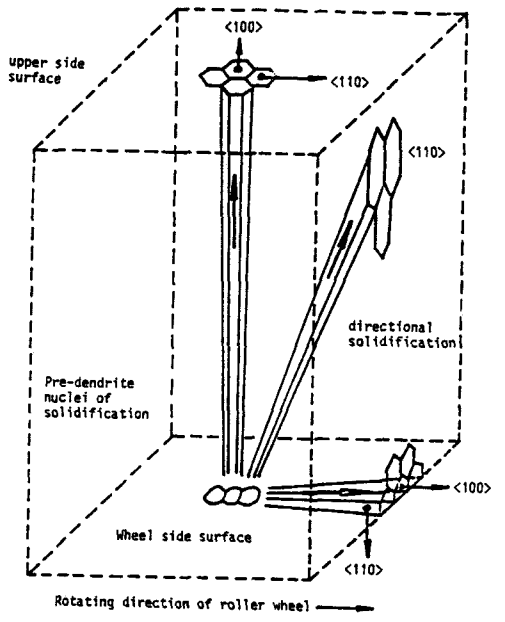

Figure 10. Schematic illustration of the solidification of the alloys, showing predendritic nuclei at the wheel-side surface and cellular-type growth emanating from the nuclei.

where λ is the dendrite arm spacing (μm), $\dot{\varepsilon}$ is the cooling rate (K 1/3) and β is a constant. Insertion of the appropriate data into the above expression suggests a cooling rate greater than $10^5 KS^{-1}$ at the wheel side surface and a cooling rate between 10^4-$10^5 KS^{-1}$ at the upper surface. Such values appear realistic for the thickness of the alloy ribbons developed, and may be compared with cooling rates of 10^6-$10^{10} KS^{-1}$ for electron transparent regions of relatively thin foils developed in gun-quenched materials (12,13).

Anodic Film Formation

Anodizing of the alloys in near neutral and acid solutions reveals behaviour which is generally typical of two phase materials, e.g. anodic film growth over the macroscopic aluminium-rich surface and local behaviour at 'second-phase' materials, often with their zone of influence into the adjacent anodic alumina film material. However, for the present alloys an almost unique situation is evident, particularly for the wheel-side surfaces, where cells of aluminium-rich material surrounded by silicon-containing material develop from a nucleus parallel to the plane of the surface. Thus, on a microscopic scale, discrete linear regions of aluminium-rich material, of effective diameters across the surface of about 0.26μm, separated from their neighbours by a continuous enveloping network of silicon-rich material, are present at the alloy surface. This morphology dominates the anodizing behaviour.

Considering initially film formation on the alloys in ammonium pentaborate solution, which on aluminium proceeds by migration of Al^{3+} outwards and OH^- or O^{2-} inwards through the pre-existing airformed film to develop a barrier-type anodic film, then the following sequence of events is envisaged:

(i) During the period of slow voltage increase with time, current is distributed between the aluminium-rich phase and silica networks resulting in limited anodic alumina film growth above the former (encouraging hydration of the outer film regions) and probably, discontinuous oxidation of the latter with associated oxygen evolution. Anodic film growth on silicon has been reported to develop with an A V^{-1} ratio of about 3.8 (14), and the local evolution of oxygen from the semiconducting film material is likely to ensure that bridging of the silicon phase by the less resistive (ionic) anodic alumina, developing by Al^{3+} egress, is hindered. Thus, in the presence of the secondary anodic process, oxygen evolution, a stage of relatively limited film growth above the aluminium rich cells persist.

Essentially, this stage is similar to that evident for film growth on conventional Al-Si alloys containing fine silicon particles (15), where complete oxidation of silicon is seen with associated oxygen evolution until such particles are bridged over by anodic alumina or isolated from the aluminium substrate by alumina film encroachment around them. In the present case, with a continuous silica-containing network, such film encroachment and particle isolaton are not possible.

(ii) The end of the early stage is expected when anodic alumina formation bridges over the anodized silicon-network; this may proceed relatively readily because of the relatively highly resistive (ionic) nature of silicon dioxide, and local gas evolution limiting the current available for film growth; however, anodic alumina bridging must withstand likely mechanical disruption from oxygen evolution.

Local heating of the solution filled channel above the silicon dioxide, through Joule heating associated with current flow across the oxide for oxygen evolution, may also contribute to enhance the rate of silicon oxidation. Additionally, any local temperature rises in the solution and an adjacent alumina film may contribute to bridging by the development of relatively voluminous hydrated alumina and/or alumina of differing extents of crystallinity (16). Subsequently anodic alumina formation proceeds relatively efficiently; however, the presence of silicon dioxide and possible regions of local hydration/change of extent of crystallinity within the anodic alumina appear to shield the aluminium-rich subatrate regions, such that local scalloping at the interface proceeds. Clearly as the alloy/film interface recedes during anodic alumina formation locally high field strengths will exist at the tips of the silicon-containing phase at the interface; whether silicon can oxidize further in the presence of an overlying region of thickening alumina is not clear. Additionally, it is apparent that electroluminescence is associated with the presence of flaws, i.e. the silicon-containing networks, in the anodic film but whether major contributions arise from oxidation of silicon, or oxygen evolution, or the development of regions of anodic alumina of different extents of crystallinity have not been clarified.

In porous anodic film forming electrolytes, where film growth proceeds by OH^-/O^{2-} ingress, and dependent on the duration of anodizing, the effect of the enveloping silicon-rich material, around the aluminium-rich phase, is more persistent than observed for the relatively thin films developed in neutral solutions. Generally, relatively low steady-state voltages are observed compared with anodizing aluminium under similar conditions, which reflects current partition between the two phases and the inability of the porous anodic alumina to bridge over the silica-containing phase. Thus, during anodizing, oxidation of the silicon phase and the aluminium-rich phase proceed; scrutiny of the alloy/film interface reveals the macroscopic scalloping developed at the aluminium-rich phase interface, which indicates a more rapid oxidation than that of the silicon-containing material. Additionally, the rates of chemical dissolution of the silicon-dioxide and anodic alumina film material appear to differ widely in the acid environment; the film sections suggest that silicon dioxide is more resistant to penetration by phosphate species, disaggregation and eventual dissolution than anodic alumina, which is likely to be influneced by the microcrystalline nature of the latter film material, with the intercrystallite magma being penetrated (17).

With the above observations in mind, development of films during anodizing of the rapidly solidified alloys in phosphoric acid can be considered. Thus, initially anodic oxidation of both phases proceeds; the generally slow rate of porous anodic film development on the aluminium-rich phase, determined by the local current

partitioned into this region, and the relatively high rate of chemical dissolution of the outer porous film regions, generate a relatively friable anodic alumina film material. Enhanced disruption of this film is apparent as a result of the local oxidation of the silicon-containing phase, to a relatively voluminous oxide which also ensures continued electrolyte access to the latter phase. The result of this is a network of the more chemically resistant silicon-dioxide reflecting the distribution of the silicon-containing material present originally within the alloy, and continuing anodic alumina growth at the appropriate region of the alloy/film interface.

In cases where lateral development of silicon dioxide is evident remote from the film/solution interface, this merly reflects the original distribution of the silicon-containing phase in the alloy. However, it is interesting that the silicon-containing material appears to be completely oxidized. This possibly suggests that the film material is finely porous, with no regular pores, as seen in anodic alumina, being observed. Such a porous nature will allow electrolyte access to the underlying aluminium-rich material and continued anodizing in regions where dendritic cells have developed parallel to the alloy surface, i.e. at the wheel-side surface; additionally, possible local disruption of the oxidized silicon containing material will allow electrolyte seepage to the aluminium-rich material.

REFERENCES

1. Waseda, Y and Aust. K.T., J. Mat. Sci., *16*, 2337, 1981.
2. Dearnley, G., Benjamin, J.D., Miller, W.S. and Wiedman, L., Corros. Sci., *16*, 717, 1976.
3. Anthony, T.R. and Cline, H.E., J. Appl. Phys., *49*, 1248, 1978.
4. Mayfield, J., Aviation Week & Space Technology, Jan. 26, p. 46 1981.
5. O'Sullivan, J.P. and Wood, G.C., Proc. Roy. Soc. London, *A317*, 511, 1970.
6. Furneaux, R.C., Thompson, G.E. and Wood, G.C. Corros. Sci., *18*, 481, 1978.
7. Biloni, H. and Chalmers B., J. Mat. Sci., *3*, 139, 1968.
8. Cliff, G. and Lorimer, G.W., J. Microscopy, *103*, 203, 1975.
9. Wernick, S. and Pinner, R., "Surface Treatment of Aluminium", Vol. 2, p. 563, Draper, Teddington, 1972.
10. Biloni, H. "Aluminium Transformation Technology and Application", Eds. C.A. Pampillo, ASM et al., p.31, Ohio, 1979.
11. Metyja, H., Gressen, B.C. and Grant, N.J., J. Inst. Metals, *68*, 30, 1968.
12. Jones, H., "Rapidly Quenched Metals", Eds., N.J. Grant and B.C. Giessen, P.1, M.I.T. Cambridge, 1976.
13. Burden, M.H. and Jones, H. Metallography, *3*, 307, 1970.
14. Schmidt, P.F. and Michel, W., J. of Electrochemical Soc., *104*, 230, 1957.
15. Shimizu, K., Thompson, G.E. and Wood, G.C., Electrochim, Acta, *27*, 245, 1982.
16. Thompson, G.E., Shimizu, K. and G.C. Wood, Nature, London, *286*, 471, 1980.
17. Alvey, C., Thompson, G.E. and Wood, G.C., "Proc. 10th World Congress on Metal Finishing" p. 275, ed. S. Haruyama, Metal Fin. Soc. Japan, Kyoto, 1980.